Whirling of a Rotor on Isotropic Shaft considering Gyroscopic Effect and Asymmetric Bearing Stiffness

C. Chattoraj[1], S.N. Sengupta[2] and M.C. Majumder[3]

[1] Assistant Professor, M.E Deptt, Dr. B.C. Roy Engg. College, Durgapur, West Bengal, India.
[2] Emeritus Scientist, R & D Centre, Dr. B.C. Roy Engg. College, Durgapur, West Bengal, India.
[3] Professor, M.E Department, NIT, Durgapur, West Bengal, India.

* Corresponding Author: (e-mail: chandanchattoraj@yahoo.co.in)

Abstract

In a variety of moving machineries ranging from tiny micro-motors to giant turbo aircraft, rotors are principal elements. Early investigators had noticed the effects of imbalance and increasing speeds on the vibrations as the rotors operated near resonance. In modern rotors, it is not unusual to consider speeds in excess of 30,000 rpm as typical since faster machines improve power-to-weight ratios. For better design and operational safety it is important to correctly understand the dynamics of the rotors. In many instances, the rotors are asymmetric and exhibit complex kinetics. Some simplification occurs when the systems are orthotropic, but they may display a number of interesting peculiarities including parametric oscillations, half-critical resonance due to gravity in horizontal rotors, etc. In the present research, the authors consider an overhanging high inertia horizontal rotor on a flexible isotropic shaft with asymmetric end bearings providing distinctly different elastic and damping characteristics in two fixed reference directions. The analysis includes the effects of rotatory inertia, gyroscopic couple, coriolis force and internal and external damping giving rise to a set of differential equations with variable coefficients where ranges of unstable operations have been noted. Digital simulation of the mathematical model, apart from exhibiting ½ critical resonance, documents irregular dynamic response of the system at certain speed and parameter combinations – the motion evolving very differently under slight changes in initial conditions.

Keywords: Asymmetric Rotor Bearing Systems; Instability; Gyroscopic Couple; Rotatory Inertia; Coriolis Force; Supercritical response.

Introduction:

Rotors are vital elements of a large number of moving machineries. Examples are varied and include machine tools, industrial turbo-machinery, aircraft gas turbine engines, tiny micro motors and many more. Vibrations caused by mass imbalance usually create much problems in rotating machinery. Imbalance occurs if the mass centre of the rotor does not coincide with its axis of rotation. Even though higher speeds induce greater centrifugal imbalance forces the current trend of higher power density invariably prefers higher operational speeds in rotating machinery. For example, speeds as high as 30,000 rpm are typical in current high-speed machining applications.

Early investigators noticed the occurrence of excessive vibrations of rotors when the speed of rotation came close to the natural frequency. This had been termed as the "critical speed". Jeffcott[(1)] in 1919 considered the lateral vibrations of a flexible shaft in the vicinity of critical speeds. In his analytical model, which consisted of a single disk assumed as a point mass, the moment of inertia was absent. Despite its simplicity, analysis of this model explained many phenomena observable in rotors. Researchers like De Laval and Föppl showed that operation beyond the critical speed is a possibility where a significant reduction of vibrations can be expected. Several studies of Jeffcott rotors have been reported by Karpenko et al[(2)] and Pavlovskaia et al[(3)]. Chattoraj, Sengupta and Majumder[(4)] considered a two dimensional isotropic and flexible horizontal rotor where the coriolis force and gravity action were considered : here the special interest was concentrated on the irregular dynamic response at the supercritical state.

Despite greatest care, rotors cannot be fully balanced dynamically and at high speeds, operative centrifugal actions tend to intensify vibrations. With nonlinear flexible systems sub-harmonic vibrations may

occur at periods that are integer multiples of the fundamental[19].

An accurate prediction of the dynamic characteristics is vital to the designer of rotating machinery. Most rotors are axisymmetric and their analysis is somewhat simpler. Some rotors, however, do not possess this symmetry with the result that much complication is introduced in their analysis. Further, rotors formed with flexible shafts with large disks, set up gyroscopic and rotatory inertia couples that introduce new and complex dynamics.

Dimentberg[5] in his well known work on Flexural Vibrations of rotating shafts covered various aspects of rotor dynamics ranging from simple central disk rotors to complex ones on flexible bearings. Critical speeds of continuous shaft-disk systems have been studied by Eshleman and Eubanks[7]. They included the effects of transverse shear, rotatory inertia and gyroscopic moments. Finite element methods were used to determine critical speeds of straight circular rotors by Nelson et. al[8, 9] and Rouch and Rao[10] . Gmur and Rodrigues[11] studied the dynamics of tapered circular rotors. The effect of shear deflection and rotary inertia on the critical speeds of the rotor was taken into account by Grybos Gliwice[6], which are of interest especially when a critical speed of higher order is concerned and the ratio of slenderness of a rotor is small.

Ozguven and Ozkan[12] presented the combined effects of shear deformation and internal damping to analyse the natural whirl speeds and unbalance response of rotor-bearing systems.

Information about the stability of vibratory motions becomes essential for ensuring better designs of rotor-bearing systems and operational safety. The effects of bearing and shaft asymmetries on the stability of the rotor has been reported by Ganesan[13]. Gunter Jr. and Trumpler[14] evaluated the stability of the single disk rotor with internal friction on damped, anisotropic supports. Wettergren and Olsson[15] considered a horizontal rotor with a flexible shaft supported in flexible bearings and found that major instabilities appear near the imbalance resonance and remarked that the resonances due to gravity near one half of the major critical could be reduced with enhanced material damping. Hull[16] experimentally scrutinized the whirling of a rotor in anisotropic bearings and also studied the backward whirling process theoretically. Smith[17], while studying the motion of an asymmetric rotor in flexible anisotropic bearings, found that the motion was marked by unstable ranges bounded by critical speeds with instabilities at speeds lower than the principal critical. Chattoraj, Sengupta and Majumder[18] also investigated the dynamics of a vertical Jeffcott rotor with a very flexible shaft whose compliance far exceeded that of the support bearings. Their analysis discussed the fascinating evolution of vibratory motion in a two dimensional model as the rotor passed from the subcritical to supercritical status.

Much attention is given by investigators to vibration of rotors as this impedes the normal service or even directly endangers the safety of the system by gradually promoting fatigue failure. The elastic vibration characteristics of rotatory systems have been reported by Panovko[19] and Biezeno and Grammel[20] – the latter work being regarded as classic. Chong-Won-Lee[21] discussed the analytical aspects of rotor dynamics ranging from simple Jeffcott rotor to multi-degree-of-freedom systems.

In the earlier cited communications, the present authors[4,18] had reported a chaos like intriguing evolution of dynamics of flexible rotors in the neighbourhood of instability. Flexible rotors have lower static rigidity but may be an important choice from the stand point of weight reduction: what is most vital is to explore the condition of smooth running of such rotors at the operating point. The intent of the present investigation into flexible rotors is to scrutinize the effects of coriolis force, gyroscopic couple and rotatory inertia on the system dynamics.

Nomenclature:

C	: Damping coefficient (translational) (N.s/m)
C_0	: Damping coefficient (rotational) (N.m-s/rad)
C_x, C_y	: Damping coefficients at the end bearing along x-axis and y- axis (N.s/m)
d	: Diameter of the shaft (m)
d_1	: Diameter of the disk (m)
F_x, F_y	: Restoring force components along x , y –axes (N)
F_{xr}, F_{yr}	: Restoring force components along x_r, y_r axes (N)
g	: Gravitational acceleration (m/s^2)
K	: Lateral bending stiffness of the shaft at disk location (N/m)
K_0	: Rotational bending stiffness of the shaft at disk location (Rad/N-m)
K_x, K_y	: End bearing stiffness along x , y- axes (N/m)
L	: Span of the horizontal cantilever shaft (m)
m	: Equivalent mass of the rotor system (kg)
p	: Natural frequency in bending (rad/s)
r_c, r_k	: Bearing property ratio (damping, stiffness)
x, y	: Non-rotating frame of reference (m)
x_r, y_r	: Rotating frame of reference (m)
$\dot{x}, \dot{y}$	: Velocity components along x- and y- axes directions respectively (m/s)
$\dot{x}_r, \dot{y}_r$	: Velocity components along x_r- and y_r- axes directions respectively (m/s)
ε	: Eccentricity of disk mass centre (m).

θ : Angular displacement at any instant of time 't' (rad)

δ : Static deflection (m) = mg/K.= g/p^2

$\gamma = \frac{\omega}{p}$: Frequency ratio

ν : Natural frequency in wobbling (rad/s)

ζ, ζ_m, ζ_0 : Damping ratios

μ_c, μ_k : Asymmetry at bearing (damping, stiffness)

τ : Acceleration time (s).

$\omega = \dot{\theta}$: Angular velocity at any instant of time 't' (rad/s)

ω_{cr} : Critical speed (rad/s)

Equations of Motion:

The mathematical model is shown in fig.1.

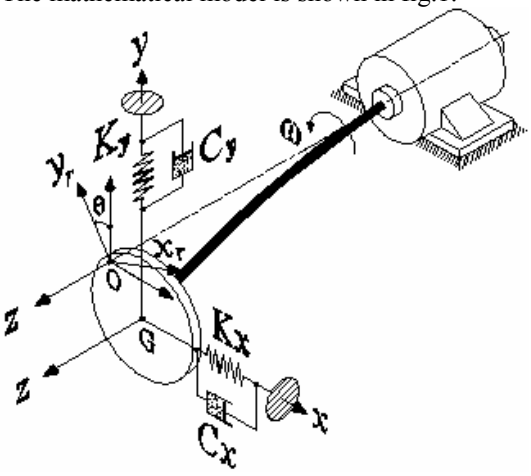

Fig.1: The Cantilever Rotor Model

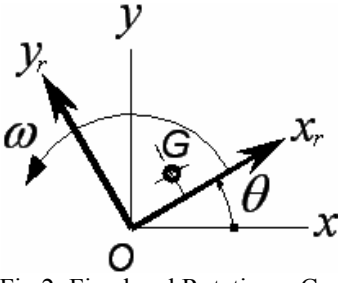

Fig.2: Fixed and Rotating Co-ordinate system

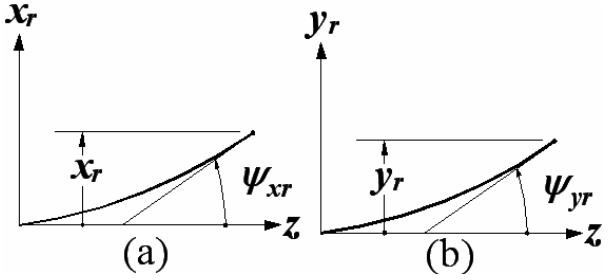

Fig.3(a, b): Snap-shot of Slope-Deflection Pattern

Fig.1 proposes the model which shows a flexible shaft rigidly supported on a bearing at one end while its other end, carrying a thin disk, is also resting against a bearing mounted flexibly. One may note that in such an arrangement, the rotating shaft provides damping and elastic restoring forces rotating with the shaft, while the flexible bearing at the disk end provides stationary elastic and damping forces. One purpose of providing a flexible support at the disk end is to act as an arrestor during resonant/unstable conditions: more importantly, the other purpose is to produce a model where the elastic and damping parameters are time variant. The fixed and the rotating coordinate systems (the reference frames) are shown in fig.2 while fig.3 (a, b) pictures the slope-deflection patterns of the elastic shaft at the disk end in the rotating x_r-z and y_r-z planes.

The co-ordinates of 'G' (the centre of mass of the disk) are expressible both in terms of the fixed and the rotating co-ordinate systems of fig.2. The following two transformation equations relate these two co-ordinate systems:

$$\begin{Bmatrix} x \\ y \end{Bmatrix} = \begin{bmatrix} \cos\theta & -\sin\theta \\ \sin\theta & \cos\theta \end{bmatrix} \begin{Bmatrix} x_r \\ y_r \end{Bmatrix} \quad \text{..... (1)}$$

and, $$\begin{Bmatrix} x_r \\ y_r \end{Bmatrix} = \begin{bmatrix} \cos\theta & \sin\theta \\ -\sin\theta & \cos\theta \end{bmatrix} \begin{Bmatrix} x \\ y \end{Bmatrix} \quad \text{.....(2)}$$

The rotating shaft-disk system shows both lateral (x_r, y_r) and rotational (ψ_{xr}, ψ_{yr}) deflections in the x_r – z and y_r – z planes respectively, as in fig.3 (a, b).

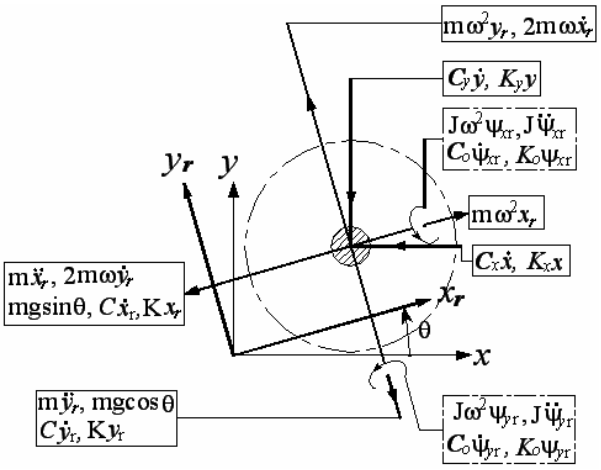

Fig.4: Forces and Moments on the Rotor System

We start with a balanced rotor with high flexibility. Modern precision rotors may be balanced to within 1 micron (eccentricity) and for a flexible horizontal rotor, the static deflection will be many times higher than this figure to justify this assumption. Also, a forward synchronous whirl is assumed. Figure 4 shows the various forces and moments acting in the $x_r - z$ and $y_r - z$ planes. The forces are identifiable as: inertia, Coriolis, centrifugal, spring, damper and gravity forces. The moments are arising from: inertia, gyroscopic, spring and damper actions. For large slope angles ψ_{xr} and ψ_{yr}, the gyroscopic moment terms shall be replaced by $J\omega^2(2\sin\psi_{xr} - 0.5\sin 2\psi_{xr})$ and $J\omega^2(2\sin\psi_{yr} - 0.5\sin 2\psi_{yr})$ in the $x_r - z$ and $y_r - z$ planes respectively.

The critical speed of a lumped mass cantilever shaft considering forward precession (gyroscopic effect)[19], is given by :

$$\omega_{cr} = \left[\frac{2EI}{ml^3}\left\{\left(3-\frac{1}{D}\right)+\sqrt{\left(3-\frac{1}{D}\right)^2+\frac{3}{D}}\right\}\right]^{1/2} \quad \ldots\ldots\ldots (3)$$

where $D = \dfrac{J}{ml^2}$

This speed is higher than the critical speed (i.e, natural frequency p) of the static cantilever.

Applying d' Alembert's principle and referring to fig.4, the equations of motion for the system (small slopes) can be written as follows in the rotating reference frame:

$$M\ddot{q} + (C_i + C_e + A)\dot{q} + (K_i + K_e + E + B + G)q = f \quad \ldots\ldots\ldots\ldots\ldots (4)$$

Where:

$$M = \begin{bmatrix} m & 0 & 0 & 0 \\ 0 & m & 0 & 0 \\ 0 & 0 & J & 0 \\ 0 & 0 & 0 & J \end{bmatrix}, \qquad C_i = \begin{bmatrix} C & 0 & 0 & 0 \\ 0 & C & 0 & 0 \\ 0 & 0 & C_0 & 0 \\ 0 & 0 & 0 & C_0 \end{bmatrix},$$

$$C_e = \begin{bmatrix} C_{11} & -C_{12} & 0 & 0 \\ -C_{12} & C_{11} & 0 & 0 \\ a_1C_{11} & -a_1C_{12} & 0 & 0 \\ -a_1C_{12} & a_1C_{11} & 0 & 0 \end{bmatrix},$$

$$A = \begin{bmatrix} 0 & 2m\omega & 0 & 0 \\ -2m\omega & 0 & 0 & 0 \\ 0 & 2a_1m\omega & 0 & 0 \\ -2a_1m\omega & 0 & 0 & 0 \end{bmatrix}$$

$$K_i = \begin{bmatrix} K & 0 & 0 & 0 \\ 0 & K & 0 & 0 \\ 0 & 0 & K_0 & 0 \\ 0 & 0 & 0 & K_0 \end{bmatrix},$$

$$K_e = \begin{bmatrix} K_{11} & -K_{12} & 0 & 0 \\ -K_{12} & K_{11} & 0 & 0 \\ a_1K_{11} & -a_1K_{12} & 0 & 0 \\ -a_1K_{12} & a_1K_{12} & 0 & 0 \end{bmatrix},$$

$$E = \omega\begin{bmatrix} -C_{12} & -C_{11} & 0 & 0 \\ C_{11} & C_{12} & 0 & 0 \\ -a_1C_{12} & -a_1C_{11} & 0 & 0 \\ a_1C_{11} & a_1C_{12} & 0 & 0 \end{bmatrix},$$

$$B = \begin{bmatrix} -m\omega^2 & 0 & 0 & 0 \\ 0 & -m\omega^2 & 0 & 0 \\ 0 & 0 & 0 & 0 \\ 0 & 0 & 0 & 0 \end{bmatrix},$$

$$G = \omega^2\begin{bmatrix} 0 & 0 & a_2J & 0 \\ 0 & 0 & 0 & a_2J \\ 0 & 0 & J & 0 \\ 0 & 0 & 0 & J \end{bmatrix}.$$

where: $q = \begin{bmatrix} x_r & y_r & \psi_{xr} & \psi_{yr} \end{bmatrix}^T$, is the generalized coordinates vector of the rotor.

f = f(t)

$= \left[-m.\sin\theta \quad -m.\cos\theta \quad -a_1 m.\sin\theta \quad -a_1 m.\cos\theta \right]^T$

, is an external forcing function vector including gravity, where $\theta = \omega t$ for uniform whirl.

$K_{11} = K_m + K_n \cos 2\theta$, $K_{12} = K_n \sin 2\theta$,

$C_{11} = C_m + C_n \cos 2\theta$, $C_{12} = C_n \sin 2\theta$,

$K_m = \frac{1}{2}\left(K_x + K_y\right)$, $K_n = \frac{1}{2}\left(K_x - K_y\right)$,

$C_m = \frac{1}{2}\left(C_x + C_y\right)$, $C_n = \frac{1}{2}\left(C_x - C_y\right)$ and a_1, a_2 are coefficients such that : force $\times .a_1$ = moment equivalent of force (producing slope) and moment $\times$ a_2 = force equivalent of moment (producing deflection).

The above equation can be expanded to the following form after some mathematics:

$$\ddot{x}_r + 2\left[\zeta p + \zeta_m p_m\left(1 + \mu_c \cos 2\theta\right)\right]\dot{x}_r + 2\left(\omega - \zeta_m p_m \mu_c \sin 2\theta\right)\dot{y}_r + \left[p^2 - \omega^2 + p_m^2\left(1 + \mu_k \cos 2\theta\right) - 2\zeta_m p_m \mu_c \omega \sin 2\theta\right]x_r - \left[\mu_k p_m^2 \sin 2\theta + 2\zeta_m p_m \omega\left(1 + \mu_c \cos 2\theta\right)\right]y_r + a_2 \rho^2 \omega^2 \psi_{xr} + g\sin\theta = 0 \quad \ldots\ldots\ldots\ldots\ldots\ldots\ldots\ldots (5)$$

Where: $p = \sqrt{\frac{K}{m}}, K = \frac{3EI}{L^3}$, $p_m = \sqrt{\frac{K_m}{m}}$,

$\mu_k = \frac{1 - r_k}{1 + r_k}$, $r_k = \frac{K_y}{K_x}$, $\mu_c = \frac{1 - r_c}{1 + r_c}$, $r_c = \frac{C_y}{C_x}$,

$\rho = \sqrt{\frac{J}{m}}$, $\zeta = \frac{C}{2\sqrt{K.m}}$, $\zeta_m = \frac{C_m}{2\sqrt{K_m.m}}$.

$$\ddot{y}_r + 2\left[\zeta p + \zeta_m p_m\left(1 - \mu_c \cos 2\theta\right)\right]\dot{y}_r - 2\left(\omega + \zeta_m p_m \mu_c \sin 2\theta\right)\dot{x}_r + \left[p^2 - \omega^2 + p_m^2\left(1 - \mu_k \cos 2\theta\right) + 2\zeta_m p_m \mu_c \omega \sin 2\theta\right]y_r - \left[\mu_k p_m^2 \sin 2\theta + 2\zeta_m p_m \omega\left(1 - \mu_c \cos 2\theta\right)\right]x_r + a_2 \rho^2 \omega^2 \psi_{yr} + g\cos\theta = 0 \quad \ldots\ldots\ldots\ldots\ldots\ldots\ldots\ldots (6)$$

$$\ddot{\psi}_{xr} + \left(\nu^2 + \omega^2\right)\psi_{xr} + 2\zeta_0 q \dot{\psi}_{xr} + \frac{2a_1}{\rho^2}\zeta_m p_m\left(1 + \mu_c \cos 2\theta\right)\dot{x}_r - \frac{2a_1}{\rho^2}\left(\omega - \zeta_m p_m \mu_c \sin 2\theta\right)\dot{y}_r + \frac{a_1}{\rho^2}\left[\omega^2 - p_m^2\left(1 + \mu_k \cos 2\theta\right) + 2\zeta_m p_m \mu_c \omega \sin 2\theta\right]x_r + \frac{2a_1}{\rho^2}\left(\omega - \zeta_m p_m \mu_c \sin 2\theta\right)\dot{y}_r - \frac{a_1 p_m}{\rho^2}\left[\mu_k p_m \sin 2\theta + 2\zeta_m \omega\left(1 + \mu_c \cos 2\theta\right)\right]y_r + \frac{a_1}{\rho^2} g\sin\theta = 0 \quad \ldots\ldots\ldots\ldots\ldots\ldots\ldots\ldots (7)$$

Where: $\zeta_0 = \frac{C_0}{2\sqrt{K_0.J}}$, $K_0 = \frac{EI}{L}$, $\nu = \sqrt{\frac{K_0}{J}}$.

$$\ddot{\psi}_{yr} + \left(\nu^2 + \omega^2\right)\psi_{yr} + 2\zeta_0 q \dot{\psi}_{yr} + \frac{2a_1}{\rho^2}\zeta_m p_m\left(1 - \mu_c \cos 2\theta\right)\dot{y}_r - \frac{2a_1}{\rho^2}\left(\omega + \zeta_m p_m \mu_c \sin 2\theta\right)\dot{x}_r - \frac{a_1}{\rho^2}\left[\omega^2 - p_m^2\left(1 - \mu_k \cos 2\theta\right) - 2\zeta_m p_m \mu_c \omega \sin 2\theta\right]y_r - \frac{a_1 p_m}{\rho^2}\left[\mu_k p_m \sin 2\theta - 2\zeta_m \omega\left(1 - \mu_c \cos 2\theta\right)\right]x_r + \frac{a_1}{\rho^2} g\cos\theta = 0 \quad \ldots\ldots\ldots\ldots\ldots\ldots\ldots\ldots (8)$$

We define the state variables :

$v_{xr} = \dot{x}_r$, $v_{yr} = \dot{y}_r$, $\Omega_{xr} = \dot{\psi}_{xr}$, $\Omega_{yr} = \dot{\psi}_{yr}$.

Now, equations (5) to (8) can be conveniently written as 8 first order differential equations, compressed into the following matrix form :

$$\{\dot{s}\} = [F]\{s\} + \{H\}u \quad \ldots\ldots\ldots\ldots\ldots\ldots\ldots\ldots (9)$$

Where,

$\{s\} = \left[s_1 \quad s_2 \quad s_3 \quad s_4 \quad s_5 \quad s_6 \quad s_7 \quad s_8\right]^T$

$= \left[v_{xr} \quad x_r \quad v_{yr} \quad y_r \quad \Omega_{xr} \quad \psi_{xr} \quad \Omega_{yr} \quad \psi_{yr}\right]^T$

$[F] = [\alpha_{ij}]_{8x8}$, and u = g.

$$\{H\} = \left[-\sin\theta \quad 0 \quad -\cos\theta \quad 0 \quad -\frac{a_1}{\rho^2}\sin\theta \quad 0 \quad -\frac{a_1}{\rho^2}\cos\theta \quad 0\right]^T$$

Elements α_{ij} of the 8 × 8 coefficient matrix are embedded in equations (5) to (8).

These first order differential equations, though unwieldy otherwise, can be numerically handled by Runge-Kutta algorithms.

Numerical Example and Digital Simulation:

To obtain the responses of the rotor system, the following representative data are chosen:

Diameter of the Disk, d_1 : 200 mm
Equivalent mass of the Shaft-Disk system, m_e : 0.488 kg.
Mass of the Disk, m : 0.445 kg.
Diameter of Shaft (Steel) ,d : ϕ 8 mm.
Length of Shaft (Steel), L : 300 mm.
Lateral Bending Stiffness of Shaft, K : 4468N/m
Rotational Stiffness of Shaft (wobble),K_0 : 134Nm/rad
M.I of Disk (diametral), J : 2.78×10^{-4} kgm^2
Natural Frequency (bending), p : 95.69 rad/s
Natural Frequency (wobble), q : 694.22 rad/s
Horizontal Stiffness of Bearing, K_x : 4468N/m
Horizontal stiffness of Bearing, K_y : r_k.Kx

Fig.5 shows the configuration of the cantilever rotor system.

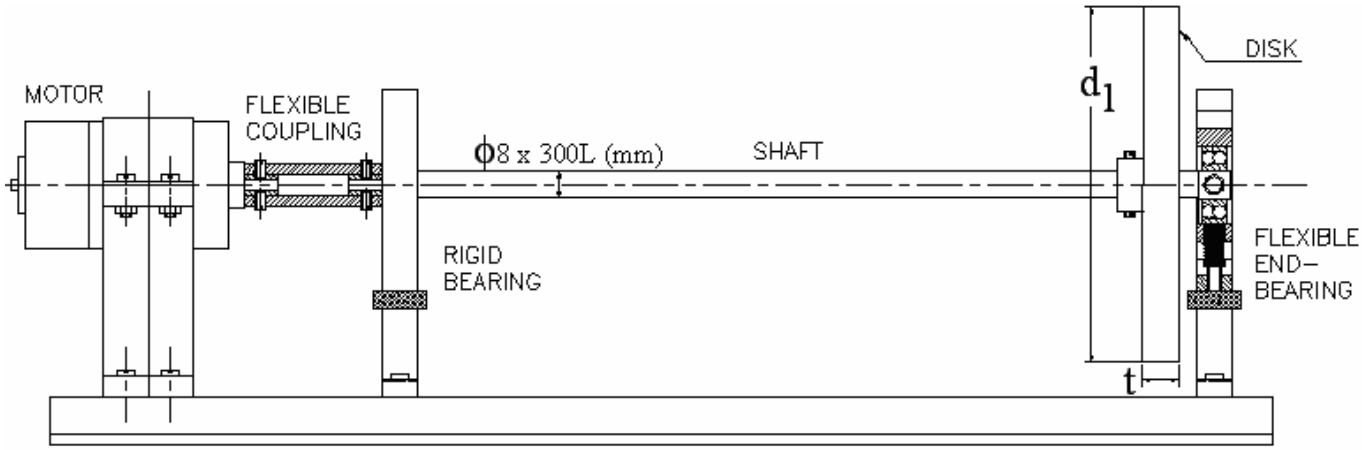

Fig.5: The Proposed Cantilever Rotor System

Results and Discussions:

Non-dimensional deflection $= \frac{x_r}{\delta}$, Frequency ratio $= \gamma = \frac{\omega}{p}$.

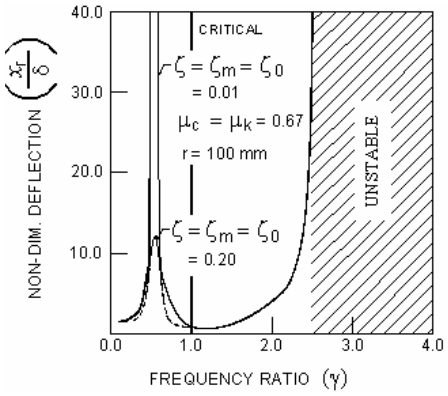

Fig.6: Stability Chart for a Rotor with Asymmetric end bearing and gyro effect.

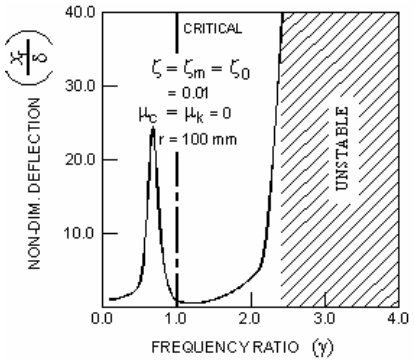

Fig.7: Stability Chart for a Rotor with symmetric end bearing and gyro effect.

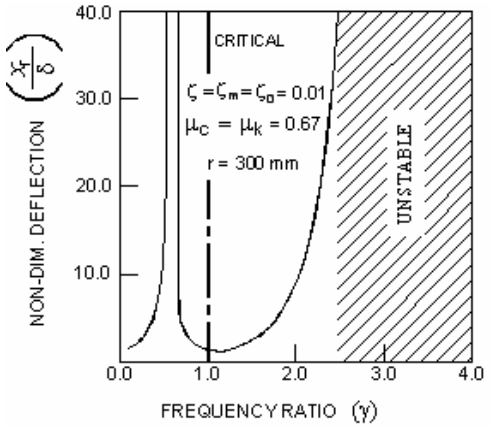

Fig.8: Stability Chart for a Rotor with Asymmetric end bearing and gyro effect.

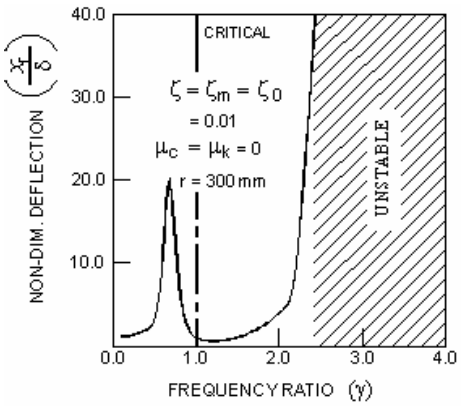

Fig.9: Stability Chart for a Rotor with symmetric end bearing and gyro effect.

Fig. 6 to fig.9 represent the stability charts plotted for two separate disk sizes and μ values.

The stability boundaries for two sets of ζ values are shown in fig.6: the case of $\zeta = \zeta_m = \zeta_0 = 0.01$ is shown in solid lines where $\mu_c = \mu_k = 2/3(\approx 0.67)$ and r =100 mm. The corresponding boundaries for $\zeta = \zeta_m = \zeta_0 = 0.2$ are given in dotted lines. In fig.6 the apparently unstable region spanning over $0.52 < \gamma < 0.63$ is a large amplitude region that matches the ½ critical resonance of horizontal rotors. The large amplitudes observed at ζ values of 0.01 can be drastically reduced to about 13 (non-dimensional) with a ζ value of 0.2. The transient response becomes unstable at $\gamma > 2.5$ (shown shaded) where damping gives little benefit.

In fig.7, a similarity with fig.6 is observable where $\mu_c = \mu_k = 0$ (isotropic end bearings). Note that the ½ critical resonance amplitude, at around $\gamma = 0.55$, is reduced to about 25. For a second order system with ζ value of 0.01, this resonance (non-dimensional) amplitude would be close to 50. The effect of symmetry in reducing amplitude is thus clear. For a disk radius of r = 100 mm, the gyro effect enhances the critical speed by 3 % over the static value, but the shift of the ½ critical point is seen to be about 10 % .

Fig.8 has features similar to fig.6. In this case, only the disk radius is changed to r = 300 mm. Though the gyro effect enhances the critical speed by 28 %, no significant change in the shape of the stability boundaries is observable except that the ½ critical resonance point is shifted by about 20 %. Similarly, fig.9 (isotropic bearings and disk radius r = 300 mm.) shows but a small change in the ½ critical resonance amplitude (reduced to around 20). The effect of gyroscopic action on the system in relation to stability is thus observed to be measly.

Notably, a resonance at $\gamma = 1$, was missed in this example, for a perfectly balanced rotor. The reason for this is to be traced in the absence of initial eccentricity ε (i.e, $\varepsilon = 0$). Since a mathematically zero eccentricity cannot be achieved mechanically, a sharp resonance line (chain-dotted) at $\gamma = 1$ is shown in fig.6, 7, 8 and 14.

In the following illustrations we represent cases of sub-critical (at $\gamma = 0.40$) to supercritical (at $\gamma = 2.50$) rotors. The damping ratios are kept small (0.01) to be compatible with material damping, and all initial values are kept zero (except fig.13(c)).

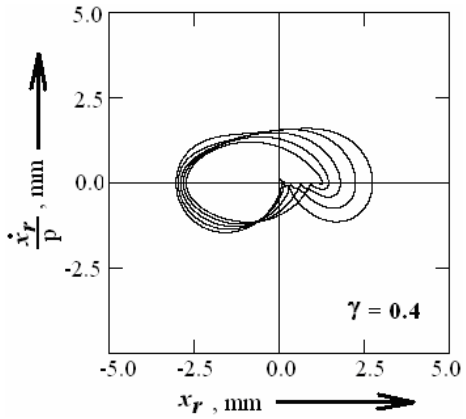

Fig.10(a): Phase-plane plot for r = 100mm, $\zeta = \zeta_0 = \zeta_m = 0.01$, $\mu_c = \mu_k = 0.67$

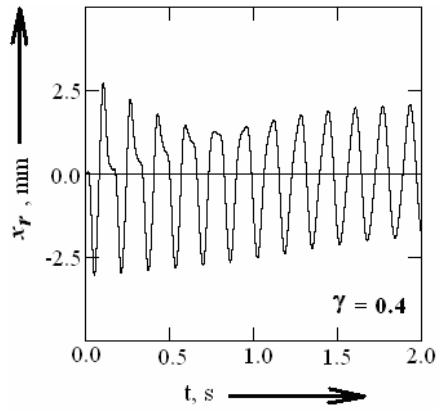

Fig.10(b): Displacement-time plot for r = 100mm, $\zeta = \zeta_0 = \zeta_m = 0.01,\ \mu_c = \mu_k = 0.67$

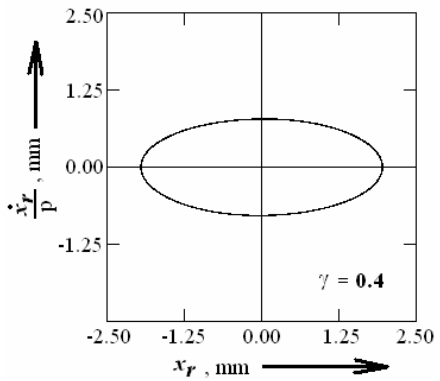

Fig.10(c): Phase-plane plot for r = 100mm, $\zeta = \zeta_0 = \zeta_m = 0.01,\ \mu_c = \mu_k = 0.67$

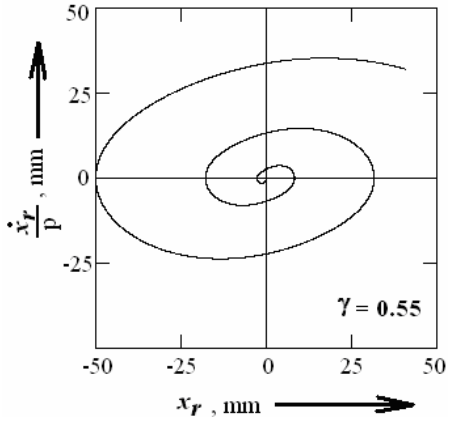

Fig.11(a): Phase-plane plot for r = 100mm, $\zeta = \zeta_0 = \zeta_m = 0.01,\ \mu_c = \mu_k = 0.67$

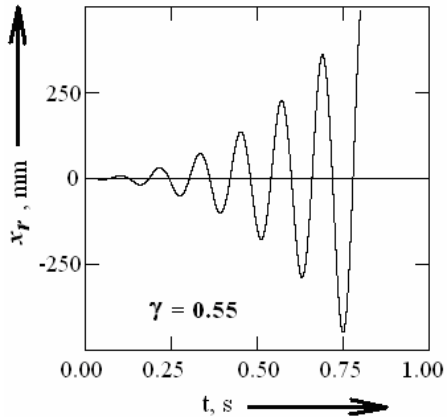

Fig.11(b): Displacement-time plot for r = 100mm, $\zeta = \zeta_0 = \zeta_m = 0.01,\ \mu_c = \mu_k = 0.67$

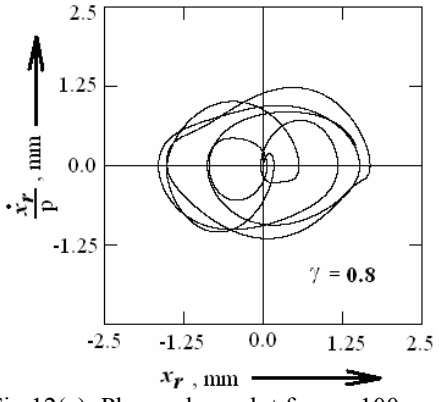

Fig.12(a): Phase-plane plot for r = 100mm, $\zeta = \zeta_0 = \zeta_m = 0.01,\ \mu_c = \mu_k = 0.67$

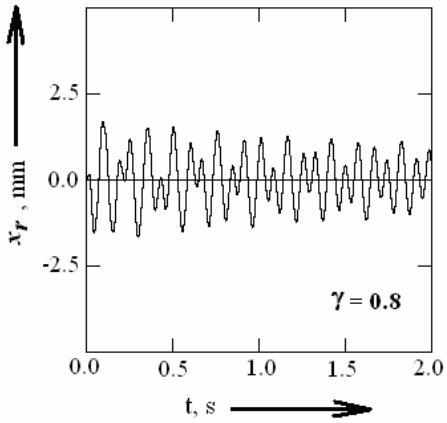

Fig.12(b): Displacement-time plot for r = 100mm, $\zeta = \zeta_0 = \zeta_m = 0.01,\ \mu_c = \mu_k = 0.67$

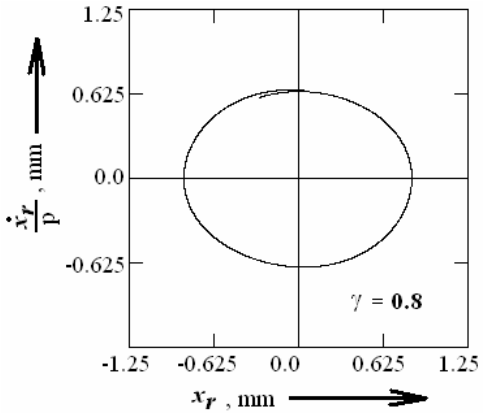

Fig.12(c): Phase-plane plot for r = 100mm, $\zeta = \zeta_0 = \zeta_m = 0.01,\ \mu_c = \mu_k = 0.67$

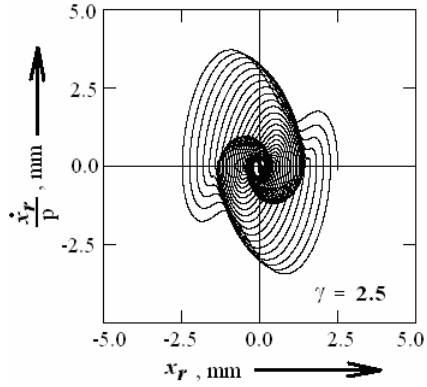

Fig.13(a): Phase-plane plot for r = 100mm, $\zeta = \zeta_0 = \zeta_m = 0.01,\ \mu_c = \mu_k = 0.67$

Fig.10(a) shows the evolution of the phase plane plot for the motion of the shaft centre along the rotating x-axis with the frequency ratio γ = 0.40 (pre ½ critical), damping ratio $\zeta = \zeta_m = \zeta_0 = 0.01$ and $\mu_c = \mu_k = 0.67$. The windings on the plot are due to a combination of harmonics at frequencies of p-ω, ω and p+ω [4]. The displacement-time graph, fig.10b, clearly shows the presence of this multiple frequency oscillations which eventually settle to one of single frequency ω due to damping of the transient at t > 2 s. In fig.10c (scale double of 10a), the phase-plane plot is constructed for t > 4 s. This elliptic figure corroborates the existence of a single frequency oscillatory motion. It is seen that a motion started with varying initial conditions settle to this trajectory in a very interesting fashion with nearly elliptic shape. The motion is stable.

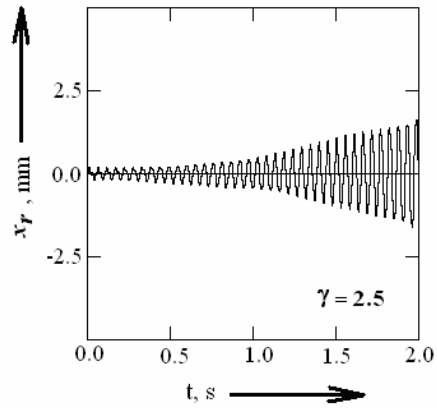

Fig.13(b): Displacement-time plot for r = 100mm, $\zeta = \zeta_0 = \zeta_m = 0.01,\ \mu_c = \mu_k = 0.67$

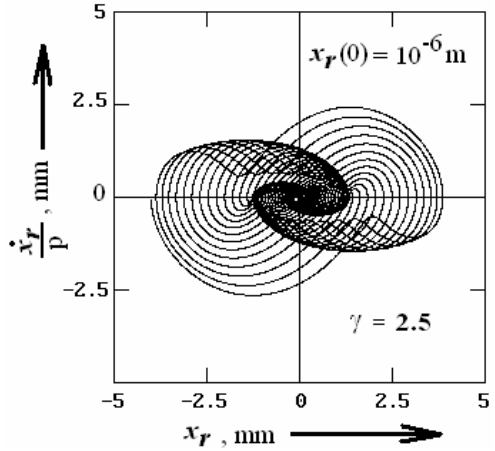

Fig.13(c): Phase-plane plot for r = 100mm, $\zeta = \zeta_0 = \zeta_m = 0.01,\ \mu_c = \mu_k = 0.67$

The phase-plane plot for γ = 0.55 is shown in fig 11(a). This motion falls in the ½ critical resonance range and the plot is seen to spiral outwards. The corresponding time history in fig.11(b), produces a rapidly diverging graph which can settle to a very large amplitude with time. Operation at this speed would be hazardous for the rotor.

Fig.12(a, b, c) represent the case of γ = 0.80 (post ½ critical state) which once again shows a cycling in an elliptic band at t > 9 s.

In fig.13(a, b, c) a super critical (γ = 2.5) state in the verge of instability is described. The phase-plane trajectory evolves in a very interesting fashion with apparent symmetry in the opposite quadrants. Fig. 13(b) shows the time history. Most interestingly, the phase-plane plot is very sensitive to initial conditions. For a slight change in initial displacement from $x_r = 0$ to $x_r = 1$ micron, the motion evolves with a notable change as in fig.13(c) where the phase-plane pattern is much altered exhibiting a

sensitive dependence to initial conditions. None of the phase paths are traversed more than once. Such features are common in chaotic systems and are not to be expected in a linear systems as this.

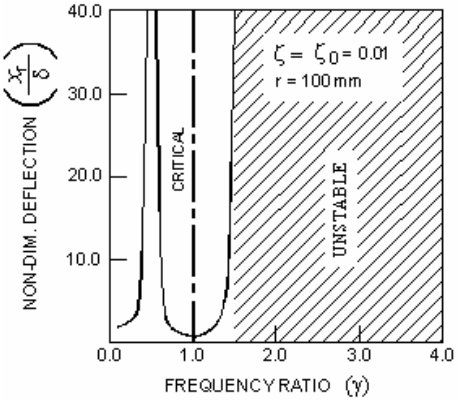

Fig.14: Stability Chart for a Cantilever Rotor

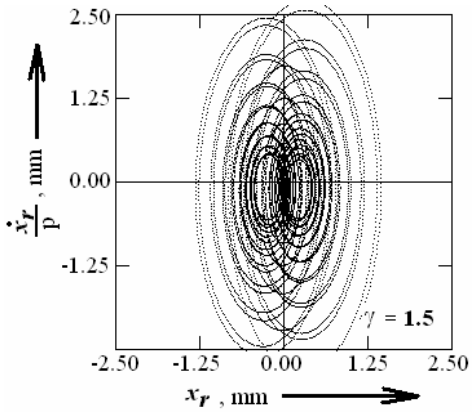

Fig.15: Phase-plane plot for cantilever , r = 100mm, $\zeta = \zeta_0 = \zeta_m = 0.01$, $\mu_c = \mu_k = 0.67$

When the end bearing is removed, the rotor becomes a free cantilever. Fig.14 shows the stability chart where a sharp ½ critical resonance is notable at $\gamma \approx 0.5$ and the system becomes unstable for γ beyond 1.5. The phase-plane plot in fig.15 ($\gamma = 1.5$) shows a twin loop spiraling pattern which, as in fig.13(a), is also in the verge of instability. Comparing fig.15 and fig.13(a) we readily realize the effect of orthotropic end support on the vibration pattern and the stability.

While constructing figs.10 to 15, the x_r-axis has been chosen for reference. If the y_r-axis were selected, like results, displaced in phase, would be obtained.

Fig.16 and 17 depict the effect of uniform acceleration time, τ to cross the ½ critical resonance zone (from 0.5p to 0.75p) on the vibration amplitude. Fig.16 shows a rapidly rising x_r (max) that moves from 2.5 mm at τ = 0.2 s to 24 mm at τ = 0.5 s. Fig. 17 shows the variation of $|x_r|$ with time, t, corresponding to τ = 0.25 s where the peak value of $|x_r|$ reads 3.6 mm. Here the ½ critical zone is crossed within **2 ¼** oscillations.

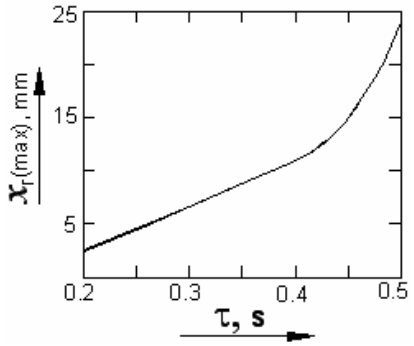

Fig.16: Variation of max. displacement

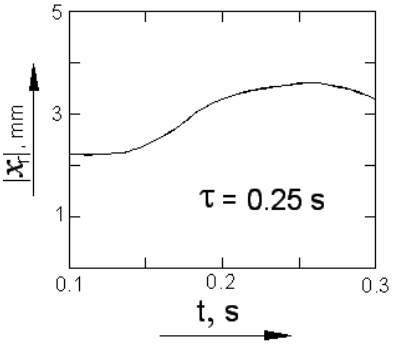

Fig.17: Variation of amplitude with time at $\tau = 0.25$ s.

Conclusions:

The phase-plane trajectories show a common feature at the sub-critical and super critical levels: the phase portraits appear as limit cycles which they are not as the same trajectory is never retraced. The present study deliberately considers a very flexible cantilever rotor with a highly compliant orthotropic bearing at the free end to reveal the effects of support resilience. Flexible rotors are preferable when weight reduction is important. A resilient end support reduces the rotor deflections and raises the range of stable operation speeds. At all events, operations near the ½ critical resonance as well as at the critical speed (γ = 1), are to be avoided as fatigue failure may soon result. In order to take the balanced flexible rotor to its supercritical operating speed, the dangerous ½ critical zone should be crossed within 2 ¼ oscillations or 0.25 s. Here the maximum vibration amplitude stays within a small value of 3.6 mm (fig.16). This implies that 100 % rotor speed should be realized within 1 s , the same requirement being also valid for deceleration. Doubtlessly, the required acceleration is high, and for a limited power

drive motor, a displacement arrestor at the end bearing becomes necessary for speeding up to the operating point.

The inclusion of gyroscopic couple, rotatory inertia and coriolis force raises the degrees of freedom of the rotor to four and the equations are formidable in structure. Contrary to expectations, however, their effects are found to be trivial in a balanced flexible (horizontal) rotor considered as an example. The results show that this rotor can be run very smoothly in the supercritical range, $1.1 < \gamma < 1.5$. The effect of the bearing asymmetry is not found to be great, excepting a marginal change in the shape of the stability chart.

Reference:

[1] H. H. Jeffcott, "*The Lateral Vibration of the Loaded Shaft in the Neighbourhood of a Whirling Speed"*, Phil. Mag., 1919, 6(37), pp 304-314.
[2] Karpenko, E., Pavlovskaia, E., and Wiercigroch, M., "*Bifurcation analysis of a preloaded Jeffcott rotor. Chaos, Solitons & Fractals"*, 2003,15(2), pp 407-416.
[3] E.E. Pavlovskaia, E.V. Karpenko and M. Wiercigroch, "*Nonlinear dynamic interactions of Jeffcott rotor with preloaded snubber ring"*, Journal of Sound and Vibration, 2004.
[4] C. Chattoraj, S.N. Sengupta and M.C. Majumder, "*Dynamic Analysis of a Rotating Shaft carrying an Axisymmetric Central Disk"*, communicated to Journal of the Brazilian Society of Mechanical Sciences and Engineering, June, 2009.
[5] F.M. Dimentberg, "*Flexural Vibrations of Rotating Shafts"*, 1961, Butterworths, London.
[6] R. Grybos, Gliwice, "*The effect of shear and rotary inertia of a rotor at its critical speeds*", Applied Mechanics, 1991, vol.61, pp 104—109.
[7] R. L. Eshleman and R. A. Eubanks, "*On the critical speeds of a continuous shaft-disk system*", Transactions of the American Society of Mechanical Engineers, Journal of Engineering for Industry, 1967, 89, pp 645-652.
[8] H. D. Nelson, "*A finite rotating shaft element using Timoshenko beam theory*", Transactions of the American Society of Mechanical Engineers, Journal of Mechanical Design, 1980 102, pp 793-803.
[9] H. D. Nelson and V. M. Mcvaugh, "*The dynamics of rotor bearing systems using finite elements*", Transactions of the American Society of Mechanical Engineers, Journal of Engineering for Industry, 1976, 102, pp 593-600.
[10] K. E. Rouch and J. S. Rao, "*A tapered beam finite element for rotor dynamics analysis*", Journal of Sound and Vibration, 1979, 66, pp 119-140.
[11] T. C. Gmur and J. D. Rodrigues, "*Shaft finite elements for rotor dynamics analysis*", Transactions of the American Society of Mechanical Engineers, Journal of Vibration and Acoustics, 1991, 113, pp 482-493.
[12] H. Nevzat Ozguven, Z. Levent Ozkan, "*Whirl speeds and unbalance response of multi-bearing rotors using finite elements*", Journal of Vibration, Acoustics, Stress, Reliability in Design, 1984,106, pp 72–79.
[13] R. Ganesan, "*Effects of bearing and shaft asymmetries on the instability of rotors operating at near-critical speeds*", Mechanism and Machine Theory, 2000, 35, pp 737-752.
[14] E. J. Gunter Jr. and P. R. Trumpler, "*The Influence of Internal Friction on the Stability of High Speed Rotors with Anisotropic Supports*", ASME Journal of Engineering for Industry, 1969, vol.91, pp 1105-1113.
[15]H.L. Wettergren and K.O. Olsson, "*Dynamic Instability of a Rotating Asymmetric Shaft with Internal Viscous Damping Supported in Anisotropic Bearings*", Journal Of Sound and Vibrations,1996,195(1), pp 75- 84.
[16]E.H.Hull, "*Shaft Whirling as Influenced by Stiffness Asymmetry*", Journal of Engineering for Industry, ASME, 1961, 83, pp 219-226
[17] D.M. Smith, "*The Motion of a Rotor Carried by a flexible Shaft in Flexible Bearings*", Proceeding of the Royal Society, 1933, ser A, 142, pp 92-118
[18] C. Chattoraj, S.N. Sengupta and M.C. Majumder, *"Dynamics of a Vertical Jeffcott Rotor"*, The Bulletin of Engineering and Science, 2008, Vol.3, No.2, pp 1-10.
[19] Ya Panovko, "*Elements of the Applied Theory of Elastic Vibrations*", Mir Pub.,Moscow, 1971, pp 161-185.
[20] C.B. Biezeno, and R Grammel, "*Engineering Dynamics*", Blackie & Son, London, 1954, pp180-259.
[21] Chong-Won Lee, "*Vibration Analysis of Rotors*", Kluwer Academic Pub.,Dordrecht, 1993, pp 1-54.
[22] C. Rajalingham, R.B. Bhat and G.D. Xistris, "*Influence of External Damping on the Stability and Resonance of a Rotor with Anisotropic Bearing Stifness*", Tribology Transactions, 1993, 36, pp 393-398.
[23] P.V. Krishnamurthy, and S.K. Sen, "*Numerical Algorithms"*, Affiliated East-West Press, New Delhi, 1986, pp 441-454.
[24] J. L. M. Morison and B. Crossland, "*An Introduction to Mechanics of Machines*", ELBS, London, 1966, pp 79-81.